2022-01

Microbial selenate detoxification linked to elemental sulfur oxidation: Independent and synergic pathways

Li, L

10.1016/j.jhazmat.2021.126932
Journal of Hazardous Materials
Elsevier BV

Microbial Selenate Detoxification Linked to Elemental Sulfur Oxidation: Independent and Synergic Pathways

Liuliu Li[a,b], Baogang Zhang[a,b*], Lei Li[a,b], Alistair G.L. Borthwick[c,d,e]

[a] *School of Water Resources and Environment, China University of Geosciences Beijing, Beijing 100083, China*

[b] *Key Laboratory of Groundwater Circulation and Evolution (China University of Geosciences Beijing), Ministry of Education, Beijing 100083, China*

[c] *St Edmund Hall, Queen's Lane, Oxford OX1 4AR, UK*

[d] *School of Engineering, The University of Edinburgh, The King's Buildings, Edinburgh EH9 3JL, UK*

[e] *School of Engineering, Computing and Mathematics, University of Plymouth, Drakes Circus, Plymouth PL4 8AA, UK*

[*] Corresponding author. Tel.: +86 10 8232 2281; Fax: +86 10 8232 1081; E-mail: baogangzhang@cugb.edu.cn (B. Zhang)

Declarations of interest: none

ABSTRACT

Elevated selenium levels in the environment, with soluble selenate [Se(VI)] as the common chemical species, pose a severe threat to human health. Anaerobic Se(VI) bioreduction is a promising approach for selenium detoxification, and various organic/inorganic electron donors have proved effective in supporting this bioprocess. Nevertheless, autotrophic Se(VI) bioreduction driven by solid inorganic electron donors is still not fully understood. This work is the first to employ elemental sulfur [S(0)] as electron donor to support Se(VI) bioreduction. A batch trial with mixed culture demonstrated the feasibility of this bioprocess, with Se(VI) removal efficiency of 92.4 ± 0.7% at an initial Se(VI) concentration of 10 mg/L within 36 h. Continuous column tests showed that increased initial concentration, flow rate, and introduction of NO_3^--N depressed Se(VI) removal. Se(VI) was mainly bioreduced to solid elemental Se with trace selenite in the effluent, while S(0) was oxidized to SO_4^{2-}. Enrichment of *Thiobacillus*, *Desulfurivibrio*, and *Sulfuricurvum* combined with upregulation of genes *serA*, *tatC*, and *soxB* indicated Se(VI) bioreduction was coupled to S(0) oxidation. *Thiobacillus* performed S(0) oxidation and Se(VI) reduction independently. Intermediate metabolites as volatile fatty acids, hydrogen, and methane from S(0) oxidation were utilized by heterotrophic Se(VI) reducers for Se(VI) detoxification, indicative of microbial synergy.

Keywords: Elemental sulfur; Selenate; Microbial reduction; Biodetoxification

1. Introduction

Selenium has an unusually narrow gap between its benefits and toxicity to humans (Lai et al., 2016). For a typical adult person, 40 to 55 μg/day of selenium is needed to support their basic nutritional needs. However, adverse impact occurs through selenosis if total selenium intake exceeds 400 μg/day (Navarro-Alarcon and Cabrera-Vique, 2008). The World Health Organization defines the selenium intake value of 40 μg/L as reference, whereas the United States Environmental Protection Agency rules that the maximum concentration of selenium must not exceed 50 μg/L in drinking water (Zhu et al., 2017; Nancharaiah et al., 2018). However, excessive concentrations of selenium are found in the environment. For example, selenium at 6000 μg/L was reported for groundwater in Utah, USA, whereas up to 9000 μg/L selenium was detected in certain areas of Colorado, USA (Ji and Wang, 2017). It is obviously important to reduce such high selenium levels below the safety threshold, especially in regions where drinking water is abstracted.

Selenate [Se(VI)] and selenite [Se(IV)] are the main forms of selenium species found in the natural aqueous environment (Latorre et al., 2013). Both Se(VI) and Se(IV) can be transformed to elemental selenium [Se(0)] enabling selenium removal due to its lower solubility, toxicity, and bioavailability (Lai et al., 2016; Song et al., 2021; Wang et al., 2021). With eco-friendly, cost-effective and in situ application advantages, microbial reduction of Se(VI) to Se(0) is preferred among remediation methods (Lenz et al., 2009; Fu et al., 2014; Qiao et al., 2018), especially with indigenous microorganisms (Li et al., 2021). Bioreduction of Se(VI) can be achieved

63 through either heterotrophic or autotrophic processes (Ontiveros-Valencia et al., 2016;
64 Zhang et al., 2019). Compared with heterotrophic metabolism, autotrophic reduction
65 is advantageous in that it prevents secondary pollution and produces less biomass,
66 making it a promising option that is also practicable and efficient (Liu et al., 2016;
67 Zhang et al., 2018).

68 Electron donors are absolutely essential in the process of autotrophic Se(VI)
69 bioreduction. For example, hydrogen (H_2) is used in gas-supported bioreduction of
70 Se(VI) (Zhou et al., 2018), but requires considerable care in its usage and storage
71 from a safety perspective. Solid inorganic electron donors that support autotrophic
72 bioreduction for metal oxyanion detoxification have also been reported (Shi et al.,
73 2019; Lu et al., 2020; He et al., 2021), of which elemental sulfur [S(0)], an insoluble,
74 stable and low-cost industrial product, has gained increasing scrutiny (Wang et al.,
75 2021). S(0) is able to serve as an electron donor for autotrophic bioprocesses
76 (Sahinkaya et al., 2014; Li et al., 2019). Many studies have explored the performance
77 of S(0) in assisting in the bioreduction of contaminants such as nitrate (NO_3^--N),
78 perchlorate (ClO_4^-), vanadate [V(V)], and chromate [Cr(VI)] (Zhang et al., 2018;
79 Ucar et al., 2019). In spite of this, autotrophic microbial Se(VI) reduction supported
80 by S(0) has been little researched, and the mechanism of Se(VI) bioreduction driven
81 by S(0) remains largely unknown.

82 Herein, bioreduction of Se(VI) supplemented by S(0) is investigated through
83 both batch and column trials, with analysis of product characterization, microbial
84 community dynamics, functional genes, and intermediate metabolites. The objectives

of this paper are: (1) to examine the feasibility and performance of S(0)-supported Se(VI) bioreduction; (2) to reveal microbial dynamics at community, gene, and metabolic levels; and (3) to analyze the mechanisms related to S(0)-driven Se(VI) bioreduction. The present study focuses on bioremediation as a potentially practicable technology for Se(VI)-polluted environments.

2. Materials and methods

2.1. Batch trial

Three groups of 250 mL volume plexiglass bottles were employed as biotic, sterilized, and abiotic batch reactors. Strict anaerobic conditions were preserved by sealing each bottle with butyl rubber stoppers and aluminum crimp caps. Before being transferred to the bottles, simulated groundwater was flushed with nitrogen gas for 30 min to remove oxygen. The biotic group with 50 mL aquifer sediment from a smelting site in China was combined with 5 g S(0) and 200 mL simulated groundwater containing the following basic constituents (g/L): $CaCl_2$ 0.2464; NH_4Cl, 0.1557; $MgCl_2{\cdot}6H_2O$, 1.0572; NaCl, 0.4459; KCl, 0.0283; KH_2PO_4, 0.0299; and $NaHCO_3$, 0.5040. The pH, ORP, and electrical conductivity of aquifer sediment were 7.99, -48.2 mV, and 424.9 μS/cm, respectively. Concentrations of organic matter and available sulphur in aquifer sediment were 34.4 g/kg and 21.9 mg/kg, respectively, whereas the cell dry weight was 6.7 mg/g soil. Concentrations of trace elements were as follows: Fe (84.2 mg/kg), Mn (2.22 mg/kg), Zn (0.19 mg/kg), Pb (0.13 mg/kg), V (0.34 mg/kg), Cr (0.33 mg/kg). The medium was supplemented with bicarbonate as

the inorganic carbon source with inorganic carbon concentration at 72 mg/L. Na_2SeO_4 was used as the source of Se(VI), at 10 mg/L concentration. All regents were purchased from Sinopharm Chemical Reagent Co., Ltd. (Beijing, China) with analytical grade, and utilized directly without further processing. The sterilized group was supplemented with S(0), simulated groundwater, and 50 mL high temperature sterilized aquifer sediment (20 min at 121 ºC). The abiotic group was supplemented with S(0) and simulated groundwater, but without aquifer sediment. All batch reactors were run for two months before data collection. The cycle of 72 h was set to evaluate Se(VI) reduction in different groups. All experiments were conducted at room temperature (22 ± 2 ºC) and in triplicate.

2.2. Column trial

A biological column of 25 cm in length and interior diameter of 5 cm was made of plexiglass. The column was covered by aluminum foil to prevent ingress of sunlight. The column was inoculated with 50 mL aquifer sediment supplemented by 200 g S(0). The remaining space was filled with quartz sand. All additives were mixed thoroughly beforehand. The synthetic water component was the same as in the batch experiment. A peristaltic pump (BT100-1L, Longer, UK) drove influent through the column at a prescribed flow rate (Zhong et al., 2011). Se(VI) and other ingredients at specified concentrations were added to the influent. The column experiment took place over 258 consecutive days divided into five phases in order to investigate the effects of different hydrodynamic and hydrochemical factors on S(0)-based Se(VI) removal (Table 1). Data were then obtained on Se(VI) removal performance, reaction

products, microbial communities, functional genes and intermediate metabolites.

2.3. Chemical analysis and characterization

Aqueous samples were filtered through 0.22 μm filter membrane, then Se(0) and the suspended microbial cells were removed by centrifuging at 12580 g for 20 min. pH, ORP, and conductivity were monitored by a multifunctional meter (SevenExcellenceS400, Mettler-Toledo, Switzerland) (Zhu et al., 2021). Inductively coupled plasma-mass spectrometry (ICP-MS, X series, Thermo Fisher, Germany) was used to determine total Se concentration. Se(IV) concentration was analyzed using a spectrophotometer (UV2300, Shanghai, China) as previously described (Li et al., 2014; Jain et al., 2015). Se(VI) was determined after being reduced to Se(IV) by hydrochloric acid (Brimmer et al., 1987; Xie et al., 2017). NO_3^--N, nitrite (NO_2^--N) and ammonium (NH_4^+-N) concentrations were also determined using spectrophotometry (Shi et al., 2020a). Ion chromatography monitored sulfate (SO_4^{2-}), sulfite (SO_3^{2-}) and thiosulfate ($S_2O_3^{2-}$) concentrations (Basic IC 792, Metrohm, Switzerland) (Shi et al., 2020b).

Analyses of the surface morphology and composition of the biomass samples were conducted using a scanning electron microscope (SEM) (JEOL JAX-840, Hitachi, Japan) equipped with energy dispersive X-ray spectroscopy (EDS). X-ray photoelectron spectroscopy (XPS) measurement was carried out to identify components of the produced deposits, using a Kratos XSAM-800 spectrometer (UK) (Zhang et al., 2012). Surface crystallographic structures of these deposits were

149 determined by X-ray diffraction (XRD) (Rigaku-D/MAX-PC 2500, Rigaku, Japan).

150 *2.4. Microbial and metabolic analyses*

151 Microbial community analysis was conducted for both inoculum and biomass
152 obtained from each stage of the biological column. Samples were collected for DNA
153 extraction, amplification, and purification, then sent to Shanghai Majorbio
154 Technology (Shanghai, China) for high-throughput 16S rRNA gene sequencing using
155 MiSeq (Illumina, USA) (Zhang et al., 2019; Wang et al., 2020). Prior to analysis,
156 centrifugation was used to remove moisture from the samples. Operational taxonomic
157 units (OTUs) were clustered from sequences with a 0.03 distance limit (equivalent to
158 97% similarity). Rarefaction curves and alpha diversity indexes were acquired by
159 Mothur (version v.1.30.1) software. Non-metric multi-dimensional scaling (NMDS)
160 analysis was performed using Bray-Curtis similarities to cluster the microbial
161 community composition.

162 Real-time quantitative PCR (qPCR) was chosen to quantify the functional genes
163 with previously reported primers (Table S1, Supporting Information) during the S(0)-
164 driven Se(VI) bioreduction process (Throbäck et al., 2004; Bru et al., 2007; Ma et al.,
165 2007; Meyer et al., 2007; Wen et al., 2016). Electron transfer compounds, such as
166 cytochrome c (Cyt c) on cell surfaces and intracellular nicotinamide adenine
167 dinucleotide (NADH), were also examined, and their measurements normalized to
168 volatile suspended solids (VSS) according to previously documented procedure
169 (Zhang et al., 2019; Shi et al., 2020a; Zhang et al., 2021). Intermediate metabolites

were also monitored. Volatile fatty acids (VFAs) were measured by a gas chromatograph (Agilent 4890, J&W Scientific, USA) equipped with a flame ionization detector (Zhang et al., 2018). A gas chromatograph (GC) (Agilent, 4890, J&W Scientific, USA) was utilized to analyze gas concentrations (including H_2 and CH_4) through a thermal conductivity detector.

3. Results and discussion

3.1. Feasibility of Se(VI) bioreduction driven by S(0)

Fig. 1a shows that a gradual, progressive decrease in Se(VI) of the biotic group occurred during the batch trial. Removal efficiency of Se(VI) reached 92.4 ± 0.7% by 36 h. Hardly any Se(VI) concentration was detected at the end of a 72 h cycle indicating almost complete removal of Se(VI). The mean reduction rate of Se(VI) was 1.1 ± 0.08 mg/L·h, corresponding to a pseudo first-order reaction kinetics process with a kinetics rate constant of 0.061 d^{-1} and R^2 of 0.99 (Fig. 1b). Temporal dynamics of Se(VI) in the control groups was also examined comparatively (Fig. S1, Supporting Information). The highest removal efficiency of Se(VI) in the sterilized group was only 18.1 ± 0.2%, much lower than that in the biotic group, suggesting Se(VI) reduction was microbially mediated. A limited Se(VI) removal efficiency of 19.1 ± 0.2% was obtained after one cycle in the abiotic group, implying that S(0) made negligible contribution to abiotic reduction of Se(VI). Taken the aforementioned into consideration, it appears quite feasible to use S(0) as an electron donor to bioreduce and biodetoxify Se(VI).

3.2. Long-term Se(VI) removal dynamics

Efficient Se(VI) elimination was observed in the column trial during 258-d operation (Fig. 1c). During Stage 1 (Days 0-94), with 10 mg/L of Se(VI) initial concentration and 0.56 mL/min constant flow rate, Se(VI) was completely removed and the corresponding Se(VI) removal capacity was 41.5 ± 4.1 ($g/m^3 \cdot d$) (Table 1). No accumulation of Se(IV) was observed during this phase. The Se(VI) removal efficiency decreased slightly to 94.1 ± 6.2% when the initial concentration of Se(VI) was raised to 50 mg/L during Stage 2 (Days 95-135), accompanied by an increase in Se(VI) removal capacity to 193.0 ± 11.9 ($g/m^3 \cdot d$). Se(VI) removal efficiency decreased to 84.2 ± 5.1% and removal capacity rose to 346.8 ± 30.2 ($g/m^3 \cdot d$) when the initial concentration of Se(VI) was further increased to 100 mg/L during Stage 3 (Days 136-176). This implied that functional microorganisms had gradually adapted to an environment characterized by high Se(VI) loading. Notably, accumulation of Se(IV) occurred for a mean concentration of 9.8 ± 15.2 mg/L, followed by almost sudden disappearance of accumulated Se(IV) at the end of Stage 3 (Fig. 1c). This phenomenon was similar to a previous study where Se(IV) accumulation was observed in Se(VI) reduction using bacterium *Bacillus sp*. SF-1 with Se(IV) removal subsequently occurring (Kashiwa et al., 2000). In Stage 4 (Days 177-217), the flow rate was adjusted to 1.68 ml/min with Se(VI) concentration returned to 10 mg/L. During this stage, Se(VI) removal efficiency increased to 89.7 ± 10.3% but the removal capacity fell to 117.0 ± 12.7 ($g/m^3 \cdot d$). In Stage 5 (Days 218-258), during which 10 mg/L NO_3^--N was introduced as co-acceptor to the bioreactor, the Se(VI) removal efficiency dropped to

82.8 ± 3.7%, suggesting that NO_3^--N was the preferred electron acceptor used by the microorganisms for metabolism, as also reported by He et al. (He et al., 2021). In a previous study, Lucas and Hollibaugh showed that Se reduction was depressed by NO_3^--N when both co-existed at equal levels owing to physiological, kinetic, or enzymatic factors involved in the NO_3^--N and Se(VI) reductases (Oremland et al., 1999; Lucas and Hollibaugh, 2001).

The evolution of pH and conductivity during long-term study were monitored. Changes in pH were in the range of 7.6 to 8.4 during the Se(VI) bioreduction process (Fig. S2, Supporting Information), with conductivity varying from 3000 to 3700 μS/cm. This ambient condition was suitable for microbial activity to achieve diverse bioprocesses (Zhang et al., 2015).

3.3. Bioprocess description

By the end of the experiment, the biological column had become dark red (Fig. S3, Supporting Information), indicating precipitation of solid Se(0) from the Se(VI) bioreduction process. The speciation percentages of selenium in the effluent were not entirely dominated by Se(VI) and Se(IV) (Fig. 2a), suggesting generation of unaccounted dissolved Se and/or organic selenium (Tan et al., 2018; Xia et al., 2019). Residual Se(VI) and Se(IV) could be further removed by adsorption or co-precipitation (Gezer et al., 2011; Li et al., 2018). To provide further confirmation of the product morphology, characterization analyses were conducted for the precipitate. In Fig. 2b, the SEM image shows spheroids observed on the surface of the biomass. EDS analysis revealed Se(0) was present in the spheroids, with a corresponding

spectral peak (Fig. S4, Supporting Information). The 56.1 eV peak signal obtained from XPS spectra relates to the 3d orbit of Se (Fig. 2c), attributed to Se(0) (Li et al., 2014). XRD demonstrated the presence of elemental Se with various crystal planes (Fig. 2d). These results collectively confirm that Se(0) was the final product in the Se(VI) bioreduction process.

SO_4^{2-} accumulated in the biosystem as a result of S(0) oxidation (Fig. 1c), indicating Se(VI) bioreduction coupled with oxidation of S(0) following Eq. (1). It should be noted that S(0) has previously been reported to act as an electron donor in the reduction of other heavy metals, accompanied by SO_4^{2-} production (Peng et al., 2016; Shi et al., 2019). SO_3^{2-} and $S_2O_3^{2-}$, the intermediates related to S(0) oxidation, were hardly detected in the present system. Moreover, hardly any NO_3^--N, NO_2^--N, and NH_4^+-N were detected at the end of Stage 5 (Fig. S5, Supporting Information), implying complete denitrification according to Eq. (2) (Zhang et al., 2015).

$$2SeO_4^{2-} + 12S^0 + 15HCO_3^- + 3NH_4^+ + H_2O \rightarrow 3C_5H_7NO_2 + 2Se^0 + 12SO_4^{2-} + 8H^+ \quad (1)$$

$$55S^0 + 20CO_2 + 50NO_3^- + 4NH_4^+ + 38H_2O \rightarrow 4C_5H_7NO_2 + 55SO_4^{2-} + 25N_2 + 64H^+ \quad (2)$$

The mass balance is calculated for Stage 4, as an example. During operation, 0.49 ± 0.05 mmol Se(VI) was removed, leading to theoretical production of 2.94 ± 0.29 mmol SO_4^{2-} according to Eq. (1). In fact, 5.15 ± 0.41 mmol SO_4^{2-} was detected, implying over-consumption of S(0), which might be ascribed to other bioactivities, such as biomass growth and the accumulation of metabolites (Shi et al., 2019).

3.4. Microbial community evolution

The evolution process of microbial community structure was examined through 16S rRNA gene sequencing for both inoculum and treated samples. OUTs in the bioreactor were lower than inoculum, indicating that the microbial community has a procedure for selection and adaptation (Table S2, Supporting Information). The decreasing total number of species (Sobs indexes) in treated samples reflected reduced community richness, which was also indicated by the Chao1 and Ace indexes. Perfect community diversity was confirmed by the lower Shannon and higher Simpson indexes in Stages 1-5, suggesting highly selected microbial communities were received (Table S2, Supporting Information). The coverage index was invariably close to unity, suggesting that almost all sequences were covered. Smooth rarefaction curves were obtained (Fig. S6, Supporting Information), confirming that the sequencing sample numbers were sufficient.

NMDS analysis showed that compared to other stages, biomass in Stage 1 was similar to the inoculum, whereas biomass from Stage 4 and Stage 5 were quite distinct from the inoculum (Fig. 3a). The microbial community composition cultivated in Stage 2 and Stage 3 were similar, which may be attributed to increased Se(VI) loading in Stage 2 that subsequently affected microorganisms in Stage 3. The Venn diagram (Fig. 3b) shows that 906, 188, 31, 188, and 449 of OTUs were found separately in five treated stages, whereas a total of 722 OTUs were common to all cultivated stages. The presence of OTUs shared by all groups implies that such OTUs had adapted simultaneously to the situations of Se(VI) bioreduction, S(0) oxidation, and NO_3^--N

279 removal.

280 Significant changes occurred in the microbial community structure of biomass
281 from the bioreactor, in comparison with the inoculum (Fig. 3c). The class related to
282 *Gammaproteobacteria* increased substantially through Stages 1 to 5, and it became
283 the predominant species (75.2%) in Stage 3. Known as NO_3^--N reducing bacteria,
284 *Gammaproteobacteria* was previously found to be the majority class in an S(0)-based
285 Cr(VI) bioreduction bioreactor (Shi et al., 2019). The *Deltaproteobacterian* species
286 increased in Stages 1 (11.1%), 2 (23.2%), 4 (34.9%), and 5 (11.3%) compared to the
287 inoculum (8.9%), but decreased in Stage 3 (7.62%). In Stage 4 especially,
288 *Deltaproteobacterian* accounted for the majority of species present. Recently, Tan et
289 al. reported that *Deltaproteobacterian* was the main community observed in their
290 study of selenium pollution wastewater microbial treatment (Tan et al., 2018).
291 Declines in both *Alphaproteobacteria* and *Actinobacteria* were observed through
292 Stages 1 to 5. *Anaerolineae* were found to be present at all treated stages. This is
293 consistent with a previous finding that bacteria related to the *Anaerolineae* family
294 have the capacity to reduce Se(VI) owing to the presence of Se(VI) reductases in
295 *Anaerolineae* (Fakra et al., 2018).

296 To develop a more profound understanding of the alteration in microbial
297 community structure, we also analyzed the relative abundance of key genera (Fig. 3d),
298 and found that the relative abundance of *Thiobacillus* increased considerably during
299 the experiment. Compared to its 0.83% abundance in the inoculum, *Thiobacillus*
300 accounted for 4.86% in Stage 1. The relative abundance of *Thiobacillus* rose to 36.8%

in Stage 2 and even higher to 72.5% in Stage 3 with elevated Se(VI) loading, and so *Thiobacillus* became the most dominant species. Although its abundance later declined, the proportion of *Thiobacillus* was 13.8% in Stage 4 and 7.31% in Stage 5. As a chemoautotrophic genus, *Thiobacillus* could oxidize S(0) to release electrons and synthesize metabolites, realizing the removal of oxidized contaminants (Yang et al., 2010; He et al., 2021). Therefore, *Thiobacillus* was believed to promote S(0) oxidation and Se(VI) reduction independently. Known as a sulfur-oxidizing bacterium, *Thiobacillus* is widely distributed in natural water, mud and soil (Fjerdingstad, 1969; Zhai et al., 2016), and thus could be utilized for the bioremediation of contaminants in practice, with high microbiological safety. Species related to *Desulfurivibrio* increased from Stages 1 to 5, with 20.8% abundance reached in Stage 4. *Desulfurivibrio* has demonstrable capability of reducing Se(VI) and Se(IV) to Se(0) without growth or respiration, using organic electron donors (Tomei et al., 1995; Lucas and Hollibaugh, 2001). And NO_3^--N can act as the terminal electron accepter of *Desulfurivibrio* in NO_3^--N dissimilatory reduction (Keith and Herbert, 1983). Other SO_4^{2-} reducing bacteria such as *Desulfococcus* and *Desulfocapsa* were detected during operation, which might be related to Se(VI) reduction and sulfur circulation (Qian et al., 2015; He et al., 2021). The relative abundance of *Pseudomonas* first declined from Stages 1 to 3, then increased in Stages 4 and 5 with proportions of 4.04% and 19.6%, respectively. Previously, reduction of Se(VI) to Se(0) was achieved using a bacterial strain belonging to *Pseudomonas*, through anaerobic respiration (Kuroda et al., 2011; Subedi et al., 2017). Although

almost none was detectable in inoculum, *Sulfuricurvum* was present in Stages 1 to 5 with respective percentages of 2.71%, 2.63%, 0.40%, 3.98% and 0.66%. As a sulfur oxidizer, *Sulfuricurvum* is known to extract energy from S(0) oxidation when synthesizing organic metabolites from an inorganic carbon source (Ontiveros-Valencia et al., 2016). *Sulfuricurvum* has also been reported capable of ClO_4^- reduction using S(0) as the electron donor (Sahu et al., 2009). *Clostridium* and *Methanobacterium* genera were also detected, with relatively lower abundances; these genera could produce H_2 and CH_4 through their metabolisms (Kamalaskar et al., 2016; He et al., 2021).

3.5. Metabolic pathway interpretation

Se(VI) was firstly reduced to Se(IV) through specialized selenate reductase (Staicu and Barton, 2021), followed by subsequent reduction of Se(IV) to Se(0) by nitrite reductase, sulfite reductase, or hydrogenase I (Harrison et al., 1984; Yanke et al., 1995; Basaglia et al., 2007). Fig. 4a shows that both *serA* and *tatC* genes were greatly enriched during Stage 1-5 despite of their concentrations were below limit of detection in the inoculum. Located in the periplasmic space, *serA* encoded specific reductase for Se(VI) bioreduction (Schröder et al., 1997; Wen et al., 2016). *tatC* was reported to encode specific enzyme capable of reducing Se(VI) (Ma et al., 2007). About twenty years ago, enzyme encoded by gene *napA* was observed to reduce Se(VI) (Sabaty et al., 2001), whereas it increased in the bioreactor rather than the inoculum in the present study. Herein, the abundance of *nirS* gene increased during Stages 1-5. Se(IV) reduction to Se(0) was attributed to the *nirS* gene because of its

345 ability to reduce Se(IV) (DeMoll-Decker and Macy, 1993); this was consistent with
346 the previously mentioned finding that there was no accumulation of Se(IV) in the
347 bioreactor. Studies also showed that nitrate/nitrite reductase genes were able to
348 accomplish the microbial reduction of vanadate (Zhang et al., 2019; He et al., 2021).
349 Encoding enzymes, gene *soxB*, related to the oxidation of S(0) to SO_4^{2-} exist at all
350 stages during operation, suggesting efficient S(0) oxidation during Se(VI)
351 bioreduction.

352 Electron transfer compounds, such as Cyt c and NADH, were found in the S(0)-
353 driven Se(VI) bioreduction system (Fig. 4b), suggesting that electron transfer
354 occurred during the S(0) oxidation and Se(VI) bioreduction bioactivities. This
355 phenomenon of electron transfer during Se(VI) biodetoxification has also been
356 reported previously (Li et al., 2021). Metabolites, including VFAs, H_2 and CH_4, were
357 also detected in the constructed biosystem (Fig. 4b). It is likely that the autotrophs
358 utilized either carbon dioxide or bicarbonate as the sole carbon source to synthesize
359 VFAs during bioreduction, with energy gained from S(0) oxidation (Estelmann et al.,
360 2011; Zhang et al., 2020). Meanwhile, VFAs have been commonly detected when
361 using H_2 and CH_4 to reduce Se(VI) (Lai et al., 2016; Ontiveros-Valencia et al., 2016).
362 VFAs, generated as the mediate product, can be utilized by heterotrophic
363 microorganisms for reduction of high-valence pollutants (Lu et al., 2020). Notably, H_2
364 and CH_4 were also detected during operation, indicating these two gases were
365 involved in the formation and/or transformation of VFAs during Se(VI) bioreduction.
366 Furthermore, these gaseous intermediate metabolites could also be utilized by Se(VI)

reducers either directly or indirectly (Lai et al., 2016; Ontiveros-Valencia et al., 2016).

3.6. Mechanism summary and practical implication

Mechanisms of Se(VI) reduction linked to S(0) oxidation can now be summarized based on the evidence obtained from the present tests (Fig. 5). Independent and synergic pathways existed for Se(VI) reduction. For the former pathway, S(0) oxidation and Se(VI) reduction could be achieved by a single chemoautotrophic genus (e.g., *Thiobacillus*). For the latter pathway, S(0) oxidizers such as *Sulfuricurvum* converted HCO_3^- to intermediate metabolites (e.g., VFAs, H_2, CH_4) as a result of S(0) oxidation, which were utilized by heterotrophic Se(VI) reducers (e.g., *Desulfurivibrio* and *Pseudomonas*). In general, dissimilatory reduction and detoxification of selenium are the main mechanisms behind Se(VI) reduction (Eswayah et al., 2016). Se(VI) bioreduction involved initial reduction of Se(VI) to Se(IV), followed by further reduction of Se(IV) to Se(0). Genes were detected that encoded specialized reductase for Se(VI) reduction to Se(IV) (i.e., *serA* and *tatC*), Se(IV) reduction to Se(0) (i.e., *nirS*), and S(0) oxidation to SO_4^{2-} (i.e., *soxB*). Electron transfer by Cyt c and NADH was verified for the Se(VI) bioreduction process.

Selenium pollution is of increasing concern due to adverse environmental impact of Se(VI). Bioremediation has been proposed as a favourable method to biotically reduce Se(VI). S(0) is readily available as a byproduct from oil refining. To our knowledge, this study is the first to report on bioreduction of Se(VI) utilizing S(0) as an electron donor, which might be a promising option for in situ bioremediation of

Se(VI) contaminated aquifers. Our finding elucidated the removal pathway where Se(VI) bioreduction can be coupled to the oxidation of S(0). In practical application, the proposed bioprocesses can be implemented with an S(0)-packed biological permeable reactive barrier installed perpendicular to the migration direction of a groundwater plume (Gibert et al., 2011). Further research can be performed to explore geological influences on the bioreduction process. Optimization of S(0) dosage is required and the effect of coexisting pollutants in aquifers, such as V(V) and SO_4^{2-}, should be considered (Du et al., 2020).

4. Conclusions

This study investigated the chemoautotrophic transformation of Se(VI) driven by S(0) in the simulated aquifer groundwater. Batch trial indicated the feasibility of Se(VI) bioreduction utilizing S(0) as an electron donor under anaerobic conditions, with Se(VI) removal efficiency of 92.4 ± 0.69% in 36 h operation. A 258-d continuous experiment showed that Se(VI) removal performance varied under different hydrodynamic and hydrochemical conditions in a column reactor. Se(VI) was reduced to insoluble Se(0) and S(0) was transformed to SO_4^{2-}. Detailed mechanisms of Se(VI) bioreduction driven by S(0) were proposed through analysis of microbial communities, functional genes, and intermediate metabolites.

Acknowledgement

This research work was supported by the National Natural Science Foundation of China (NSFC) (No. 42022055).

Reference

Basaglia, M., Toffanin, A., Baldan, E., Bottegal, M., Shapleigh, J.P., Casella, S., 2007. Selenite-reducing capacity ofthe copper-containing nitrite reductase of *Rhizobium sullae*. FEMS Microbiol. Lett. 269, 124-130.

Brimmer, S.P., Fawcett, W.R., Kulhavy, K.A., 1987. Quantitative reduction of selenate ion to selenite in aqueous samples. Anal. Chem. 59, 1470-1471.

Bru, D., Sarr, A., Philippot, L., 2007. Relative abundances of *Proteobacterial* membrane-bound and periplasmic nitrate reductases in selected environments†. Appl. Environ. Microb. 73, 5971-5974.

DeMoll-Decker, H., Macy, J.M., 1993. The periplasmic nitrite reductase of *Thauera selenatis* may catalyze the reduction of selenite to elemental selenium. Arch. Microblol. 160, 241-247.

Du, J., Zhang, B., Li, J., Lai, B., 2020. Decontamination of heavy metal complexes by advanced oxidation processes: A review. Chin. Chem. Lett. 31, 2575-2582.

Estelmann, S., Hügler, M., Eisenreich, W., Werner, K., Berg, I.A., Ramos-Vera, W.H., Say, R.F., Kockelkorn, D., Gad′on, N., Fuchs, G., 2011. Labeling and enzyme studies of the central carbon metabolism in *Metallosphaera sedula*$^{\triangledown}$. J. Bacteriol. 193, 1191-200.

Eswayah, A.S., Smith, T.J., Gardiner, P.H.E., 2016. Microbial transformations of selenium species of relevance to bioremediation. Appl. Enviro. Microb. 82, 4848-4859.

Fakra, S.C., Luef, B., Castelle, C.J., Mullin, S.W., Williams, K.H., Marcus, M.A.,

Schichnes, D., Banfield, J.F., 2018. Correlative cryogenic spectro-microscopy to investigate Selenium bioreduction products. Environ. Sci. Technol. 52, 503-512.

Fjerdingstad, E., 1969. Bacterial corrosion of concrete in water. Water Res. 3, 21-30.

Fu, Y., Wang, J., Liu, Q., Zeng, H., 2014. Water-dispersible magnetic nanoparticle-graphene oxide composites for selenium removal. Carbon 77, 710-721.

Gezer, N., Gulfen, M., Aydin, A.O., 2011. Adsorption of selenite and selenate ions onto thiourea-formaldehyde resin. J. Appl. Polym. Sci. 122, 1134-1141.

Gibert, O., Rötting, T., Cortina, J.L., Pablo, J., Ayora, C., Carrera, J., Bolzicco, J., 2011. In-situ remediation of acid mine drainage using a permeable reactive barrier in Aznalcóllar (Sw Spain). J. Hazard. Mater. 191, 287-295.

Harrison, G., Curie, C., Laishley, E.J., 1984. Purification and characterization ofan inducible dissimilatory type sulphite reductase from *Clostridium pasteurianum*. Arch. Microbiol. 138, 72-78.

He, C., Zhang, B., Lu, J., Qiu, R., 2021. A newly discovered function of nitrate reductase in chemoautotrophic vanadate transformation by natural mackinawite in aquifer. Water Res. 189, 116664.

Jain, R., Jordan, N., Weiss, S., Foerstendorf, H., Heim, K., Kacker, R., Hübner, R., Kramer, H., Hullebusch, E.D.V., Farges, F., Lens, P.N.L., 2015. Extracellular polymeric substances govern the surface charge of biogenic elemental selenium nanoparticles. Environ. Sci. Technol. 49, 1713-1720.

Ji, Y., Wang, Y.T., 2017. Selenium Reduction by Batch Cultures of *Escherichia coli* Strain EWB32213. J. Environ. Eng. 143, 1-7.

Kamalaskar, L., Kapse, N., Pore, S., Dhakephalkar, A.P., Ranade, D.R., Dhakephalkar, P.K., 2016. Genome sequence and gene expression studies reveal novel hydrogenases mediated hydrogen production by *Clostridium biohydrogenum* sp. nov., MCM B-509T. Int. J. Hydrogen Energ. 41, 11990-11999.

Kashiwa, M., Nishimoto, S., Takahashi, K., Ike, M., Fujita, M., 2000. Factors affecting soluble selenium removal by a selenate-reducing bacterium *Bacillus sp*. SF-1. J. Biosci. Bioeng. 89, 528-533.

Keith, S.M., Herbert, R.A., 1983. Dissimilatory nitrate reduction by a strain of *Desulfovibrio desulfuricans*. FEMS Microbiol. Lett. 18, 55-59.

Kuroda, M., Notaguchi, E., Sato, A., Yoshioka, M., Hasegawa, A., Kagami, T., Narita, T., Yamashita, M., Sei, K., Soda, S., Ike, M., 2011. Characterization of *Pseudomonas stutzeri* NT-I capable of removing soluble selenium from the aqueous phase under aerobic conditions. J. Biosci. Bioeng. 112, 259-264.

Lai, C.Y., Wen, L.L., Shi, L.D., Zhao, K.K., Wang, Y.Q., Yang, X., Rittmann, B.E., Zhou, C., Tang, Y., Zheng, P., Zhao, H.P., 2016. Selenate and nitrate bioreductions using methane as the electron donor in a membrane biofilm reactor. Environ. Sci. Technol. 50, 10179-10186.

Latorre, C.H., Garcia, J.B., Martin, S.G., Crecente, R.M.P., 2013. Solid phase extraction for the speciation and preconcentration of inorganic selenium in water samples: a review. Anal. Chim. Acta 804, 37-49.

Lenz, M., Enright, A.M., O'Flaherty, V., van Aelst, A.C., Lens, P.N.L., 2009.

476 Bioaugmentation of UASB reactors with immobilized *Sulfurospirillum barnesii*
477 for simultaneous selenate and nitrate removal. Appl. Microbial. Biot. 83, 377-
478 388.
479 Li, D.B., Cheng, Y.Y., Wu, C., Li, W.W., Li, N., Yang, Z.C., Tong, Z.H., Yu, H.Q.,
480 2014. Selenite reduction by *Shewanella oneidensis* MR-1 is mediated by
481 fumarate reductase in periplasm. Sci. Rep. 4, 3735.
482 Li, Y., Guo, X., Dong, H., Luo, X., Guan, X., Zhang, X., Xia, X., 2018. Selenite
483 removal from groundwater by zero-valent iron (ZVI) in combination with
484 oxidants. Chem. Eng. J. 345, 432-440.
485 Li, K., Guo, J., Li, H., Han, Y., Chen, Z., Song, Y., Xing, Y., Zhang, C., 2019. A
486 combined heterotrophic and sulfur-based autotrophic process to reduce high
487 concentration perchlorate via anaerobic baffled reactors: Performance
488 advantages of a step-feeding strategy. Bioresource Technol. 279, 297-306.
489 Li, L., Zhang, B., He, H., Zhang, H., 2021. Hydrodynamics- and hydrochemistry-
490 affected microbial selenate reduction in aquifer: Performance and mechanisms.
491 Sci. Total Environ. 768, 145331.
492 Liu, Y., Peng, L., Ngo, H.H., Guo, W., Wang, D., Pan, Y., Sun, J., Ni, B.J., 2016.
493 Evaluation of nitrous oxide emission from sulfide- and sulfur-based autotrophic
494 denitrification processes. Environ. Sci. Technol. 50, 9407-9415.
495 Lu, J., Zhang, B., He, C., Borthwick, A.G.L., 2020. The role of natural Fe(II)-bearing
496 minerals in chemoautotrophic chromium (VI) bio-reduction in groundwater. J.
497 Hazard. Mater. 389, 121911.

Lucas, F.S., Hollibaugh, J.T., 2001. Response of sediment bacterial assemblages to selenate and acetate amendments. Environ. Sci. Technol. 35, 528-534.

Ma, J., Kobayashi, D.Y., Yee, N., 2007. Chemical kinetic and molecular genetic study of selenium oxyanion reduction by *Enterobacter cloacae* SLD1a-1. Environ. Sci. Technol. 41, 7795-7801.

Meyer, B., Imhoff, J.F., Kuever, J., 2007. Molecular analysis of the distribution and phylogeny of the *soxB* gene among sulfur-oxidizing bacteria-evolution of the Sox sulfur oxidation enzyme system. Environ. Microbiol. 9, 2957-2977.

Nancharaiah, Y.V., Sarvajith, M., Lens, P.N.L., 2018. Selenite reduction and ammoniacal nitrogen removal in an aerobic granular sludge sequencing batch reactor. Water Res. 131, 131-141.

Navarro-Alarcon, M., Cabrera-Vique, C., 2008. Selenium in food and the human body: a review. Sci. Total Environ. 400, 115-141.

Ontiveros-Valencia, A., Penton, C.R., Krajmalnik-Brown, R., Rittmann, B.E., 2016. Hydrogen-fed biofilm reactors reducing selenate and sulfate: community structure and capture of elemental selenium within the biofilm. Biotechnol. Bioeng. 113, 1736-1744.

Oremland, R.S., Blum, J.S., Bindi, A.B., Dowdle, P.R., Herbel, M., Stolz, J.F., 1999. Simultaneous reduction of nitrate and selenate by cell suspensions of selenium-respiring bacteria. Appl. Environ. Microb. 65, 4385-4392.

Peng, L., Liu, Y., Gao, S.H., Chen, X., Ni, B.J., 2016. Evaluating simultaneous chromate and nitrate reduction during microbial denitrifification processes.

Water Res. 89, 1-8.

Qian, J., Liu, R., Wei, L., Lu, H., Chen, G.H., 2015. System evaluation and microbial analysis of a sulfur cycle-based wastewater treatment process for co-treatment of simple wet flue gas desulfurization wastes with freshwater sewage. Water Res. 80, 189-199.

Qiao, J., Song, Y., Sun, Y., Guan, X., 2018. Effect of solution chemistry on the reactivity and electron selectivity of zerovalent iron toward Se(VI) removal. Chem. Eng. J. 353, 246-253.

Sabaty, M., Avazeri, C., Pignol, D., Vermeglio, A., 2001. Characterization of the reduction of selenate and tellurite by nitrate reductases. Appl. Environ. Microb. 67, 5122-5126.

Sahinkaya, E., Kilic, A., 2014. Heterotrophic and elemental-sulfur-based autotrophic denitrifification processes for simultaneous nitrate and Cr(VI) reduction. Water Res. 50, 278-286.

Sahu, A.K., Conneely, T., Nüsslein, K.R., Ergas, S.J., 2009. Biological perchlorate reduction in packed bed reactors using elemental sulfur. Environ. Sci. Technol. 43, 4466-4471.

Schröder, I., Rech, S., Krafft, T., Macy, J.M., 1997. Purification and characterization of the selenate reductase from *Thauera selenatis*. J. Biol. Chem. 272, 23765-23768.

Shi, C., Cui, Y., Lu, J., Zhang, B., 2020. Sulfur-based autotrophic biosystem for efficient vanadium (V) and chromium (VI) reductions in groundwater. Chem.

542 Eng. J. 395, 124972.
543 Shi, J., Zhang, B., Cheng, Y., Peng, K., 2020a. Microbial vanadate reduction coupled
544 to co-metabolic phenanthrene biodegradation in groundwater. Water Res. 168,
545 116354.
546 Shi, J., Zhang, B., Qiu, R., Lai, C., Jiang, Y., He, C., Guo, J., 2019. Microbial
547 chromate reduction coupled to anaerobic oxidation of elemental sulfur or
548 zerovalent iron. Environ. Sci. Technol. 53, 3198-3207.
549 Shi, et al., Zhang, B., Wang, Y., Fu, J., 2020b. Effects of hydropower dam
550 construction on sulfur distribution andsulfate-reducing prokaryotes assemblage.
551 Sci. Total Environ. 705, 135819.
552 Song, B., Tian, Z., Weijden, R.D., Buisman, C.J.N., Weijma, B.J., 2021. High-rate
553 biological selenate reduction in a sequencing batch reactor for recovery of
554 hexagonal selenium. Water Res. 193, 116855.
555 Staicu, L.C., Barton, L.L., 2021. Selenium respiration in anaerobic bacteria: Does
556 energy generation pay off? J. Inorg. Biochem. 222, 111509.
557 Subedi, G., Taylor, J., Hatam, I., Baldwin, S.A., 2017. Simultaneous selenate
558 reduction and denitrification by a consortium of enriched mine site bacteria.
559 Chemosphere 183, 536-545.
560 Tan, L.C., Nancharaiah, Y.V., Lu, S., Hullebusch, E.D.V., Gerlach, R., Lens, P.N.L.,
561 2018. Biological treatment of selenium-laden wastewater containing nitrate and
562 sulfate in an upflow anaerobic sludge bed reactor at pH 5.0. Chemosphere 211,
563 684-693.

564 Tan, L.C., Papirio, S., Luongo, V., Nancharaiah, Y.V., Cennamo, P., Esposito, G.,
565 Hullebusch, E.D.V., Lens, P.N.L., 2018. Comparative performance of anaerobic
566 attached biofilm and granular sludge reactors for the treatment of model mine
567 drainage wastewater containing selenate, sulfate and nickel. Chem. Eng. J. 345,
568 545-555.
569 Throbäck, I.N., Enwall, K., Jarvis, Å., Hallin, S., 2004. Reassessing PCR primers
570 targeting *nirS*, *nirK* and *nosZ* genes for community surveys of denitrifying
571 bacteria with DGGE. FEMS Microbiol. Ecol. 49, 401-417.
572 Tomei, F.A., Barton, L.L., Lemanski, C.L., Zocco, T.G., Fink, N.H., Sillerud, L.O.,
573 1995. Transformation of selenate and selenite to elemental selenium by
574 *Desulfovibrio desulfuricans*. J. Ind. Microbiol. Biot. 14, 329-336.
575 Ucar, D., Sahinkaya, E., Yilmaz, T., Cakmak, Y., 2019. Simultaneous nitrate and
576 perchlorate reduction in an elemental sulfur-based denitrifying membrane
577 bioreactor. Int. Biodeter. Biodegr. 144, 104741.
578 Wang, S., Zhang, B., Li, T., Li, Z., Fu, J., 2020. Soil vanadium(V)-reducing related
579 bacteria drive community response to vanadium pollution from a smelting plant
580 over multiple gradients. Environ. Int. 138, 105630.
581 Wang, Y., Lai, C.Y., Wu, M., Song, Y., Hu, S., Yuan, Z., Guo, J., 2021. Roles of
582 oxygen in methane-dependent selenate reduction in a membrane biofilm reactor:
583 stimulation or suppression. Water Res. 198, 117150.
584 Wang, Z., Zhang, B., He, C., Shi, J., Wu, M., Guo, J., 2021. Sulfur-based mixotrophic
585 vanadium (V) bio-reduction towards lower organic requirement and sulfate

586 accumulation. Water Res. 189, 116655.
587 Wen, L.L., Lai, C.Y., Yang, Q., Chen, J.X., Zhang, Y., Ontiveros-Valencia, A., Zhao,
588 H.P., 2016. Quantitative detection of selenate-reducing bacteria by real-time
589 PCR targeting the selenate reductase gene. Enzyme Microb. Tech. 85, 19-24.
590 Xia, S., Xu, X., Zhou, L., 2019. Insights into selenate removal mechanism of
591 hydrogen-based membrane biofilm reactor for nitrate-polluted groundwater
592 treatment based on anaerobic biofilm analysis. Ecotox. Environ. Safe. 178, 123-
593 129.
594 Xie, Y., Dong, H., Zeng, G., Zhang, L., Cheng, Y., Hou, K., Jiang, Z., Zhang, C.,
595 Deng, J., 2017. The comparison of Se(IV) and Se(VI) sequestration by nanoscale
596 zero-valent iron in aqueous solutions: The roles of solution chemistry. J. Hazard.
597 Mater. 338, 306-312.
598 Yang, Z.H., StoVen, K., Haneklaus, S., Singh, B.R., Schnug, E., 2010. Elemental
599 sulfur oxidation by *Thiobacillus spp*. and aerobic heterotrophic sulfur-oxidizing
600 bacteria. Pedosphere 20, 7-79.
601 Yanke, L.J., Bryant, R.D., Laishley, E.J., 1995. Hydrogenase I of *Clostridium*
602 *pasteurianum* functions as a novel selenite reductase. Anaerobe 1, 61-67.
603 Zhai, J., Rahaman, M.H., Chen, X., Xiao, H., Liao, K., Li, X., Duan, C., Zhang, B.,
604 Tao, G., John, T., Vymazal, J., 2016. New nitrogen removal pathways in a full-
605 scale hybrid constructed wetland proposed from high-throughput sequencing and
606 isotopic tracing results. Ecol. Eng. 97, 434-443.
607 Zhang, B., Cheng, Y., Shi, J., Xing, X., Zhu, Y., Xu, N., Xia, J., Borthwick, A.G.L.,

2019. Insights into interactions between vanadium (V) bio-reduction and pentachlorophenol dechlorination in synthetic groundwater. Chem. Eng. J. 375, 121965.

Zhang, B., Feng, C., Ni, J., Zhang, J., Huang, W., 2012. Simultaneous reduction of vanadium (V) and chromium (VI) with enhanced energy recovery based on microbial fuel cell technology. J. Power Sources 204, 34-39.

Zhang, B., Li, Y., Fei, Y., Cheng, Y., 2021. Novel pathway for vanadium(V) bio-detoxification by Gram-positive *Lactococcus raffinolactis*. Environ. Sci. Technol. 55, 2121-2131.

Zhang, B., Qiu, R., Lu, L., Chen, X., He, C., Lu, J., Ren, Z.J., 2018. Autotrophic vanadium(V) bioreduction in groundwater by elemental sulfur and zerovalent Iron. Environ. Sci. Technol. 52, 7434-7442.

Zhang, B., Tian, C., Liu, Y., Hao, L., Liu, Y., Feng, C., Liu, Y., Wang, Z., 2015. Simultaneous microbial and electrochemical reductions of vanadium (V) with bioelectricity generation in microbial fuel cells. Bioresource Technol. 179, 91-97.

Zhang, B., Wang, S., Diao, M., Fu, J., Xie, M., Shi, J., Liu, Z., Jiang, Y., Cao, X., Borthwick, A.G.L., 2019. Microbial community responses to vanadium distributions in mining geological environments and bioremediation assessment. J. Geophys. Res-Biogeo. 124, 601-615.

Zhang, B., Wang, Z., Shi, J., Dong, H., 2020. Sulfur-based mixotrophic bio-reduction for efficient removal of chromium (VI) in groundwater. Geochim. Cosmochim.

630 Ac. 268, 296-309.
631 Zhang, L., Zhang, C., Hu, C., Liu, H., Bai, Y., Qu, J., 2015. Sulfur-based mixotrophic
632 denitrification corresponding to different electron donors and microbial profiling
633 in anoxic fluidized-bed membrane bioreactors. Water Res. 85, 422-431.
634 Zhang, Y., Kuroda, M., Arai, S., Kato, F., Inoue, D., Ike, M., 2019. Biological
635 treatment of selenate-containing saline wastewater by activated sludge under
636 oxygen-limiting conditions. Water Res. 154, 327-335.
637 Zhong, C., Zhang, B., Kong, L., Xue, A., Ni, J., 2011. Electricity generation
638 frommolasses wastewater by an anaerobic baffled stacking microbial fuel cell. J.
639 Chem. Technol. Biot. 86, 406-413.
640 Zhou, L., Xu, X., Xia, S., 2018. Effects of sulfate on simultaneous nitrate and selenate
641 removal in a hydrogen-based membrane biofifilm reactor for groundwater
642 treatment: Performance and biofifilm microbial ecology. Chemosphere 211, 254-
643 260.
644 Zhu, L., Zhang, L., Li, J., Zhang, D., Chen, L., Sheng, D., Yang, S., Xiao, C., Wang,
645 J., Chai, Z., Albrecht-Schmitt, T.E., Wang, S., 2017. Selenium sequestration in a
646 cationic layered rare earth hydroxide: a combined batch experiments and EXAFS
647 investigation. Environ. Sci. Technol. 51, 8606-8615.
648 Zhu, F., Zheng, Y.M., Zhang, B.G., Dai. Y.R., 2020. A critical review on the
649 electrospun nanofibrous membranes for the adsorption of heavy metals in water
650 treatment. J. Hazard. Mater. 401, 123608.
651

652 **Figure Captions.**

653 **Fig. 1.** Se(VI) removal performance in S(0)-driven Se(VI) reduction biosystems. (a)
654 Time histories of Se(VI) removal efficiency during three consecutive operating cycles
655 during batch trial; (b) Pseudo first-order kinetic plots for Se(VI) removal; (c) Time
656 histories of Se(VI), NO_3^--N in influent, Se(VI), Se(IV), NO_3^--N, and SO_4^{2-} in effluent,
657 corresponding Se(VI) and NO_3^--N removal efficiencies, and Se(VI) removal capacities
658 during 258 d operation of the column trial.

659 **Fig. 2.** Characterization of products from Se(VI) bioreduction. (a) Selenium speciation
660 percentages in the effluent. (b) SEM, (c) XPS, and (d) XRD analysis of the precipitates
661 after reaction. SEM: Scanning electron microscope; XPS: X-ray photoelectron
662 spectroscopy; XRD: X-ray diffraction.

663 **Fig. 3.** Microbial community evolution in inoculum and at different stages of column
664 trial. (a) Non-metric multidimensional scaling (NMDS) plot for the distribution of
665 microbial community; (b) Venn plot of microbial richness (b); (c) Class-level relative
666 abundance; (d) Heatmap of functional genera.

667 **Fig. 4.** Metabolic processes of S(0)-driven Se(VI) bioreduction. (a) Abundances of
668 functional genes; (b) Contents of electron transfer compounds and intermediate
669 metabolites. Cyt c: Cytochrome c; NADH: Nicotinamide adenine dinucleotide; VFAs:
670 Volatile fatty acids.

671 **Fig. 5.** Mechanistic pathways of microbial Se(VI) reduction processes linked to S(0)
672 oxidation. VFAs: Volatile fatty acids.

673

Table 1. Ambient conditions and Se(VI) removal performance for each stage during 258-d operation in column trial.

Stage	Period (d)	Flow rate (mL/min)	Initial Se(VI) (mg/L)	Initial NO_3^--N (mg/L)	Se(VI) removal efficiency (%)	Se(VI) removal capacity (g/(m^3/d))	NO_3^--N removal efficiency (%)	NO_3^--N removal capacity (g/(m^3/d))
1	0-94	0.56	10	-	98.1 ± 6.3	41.5 ± 4.1	-	-
2	95-135	0.56	50	-	94.1 ± 6.2	193.0 ± 11.9	-	-
3	136-176	0.56	100	-	84.2 ± 5.1	346.8 ± 30.2	-	-
4	177-217	1.68	10	-	89.7 ± 10.3	117.0 ± 12.7	-	-
5	218-258	0.56	10	10	82.8 ± 3.7	35.2 ± 2.1	97.9 ± 0.8	40.6 ± 3.3

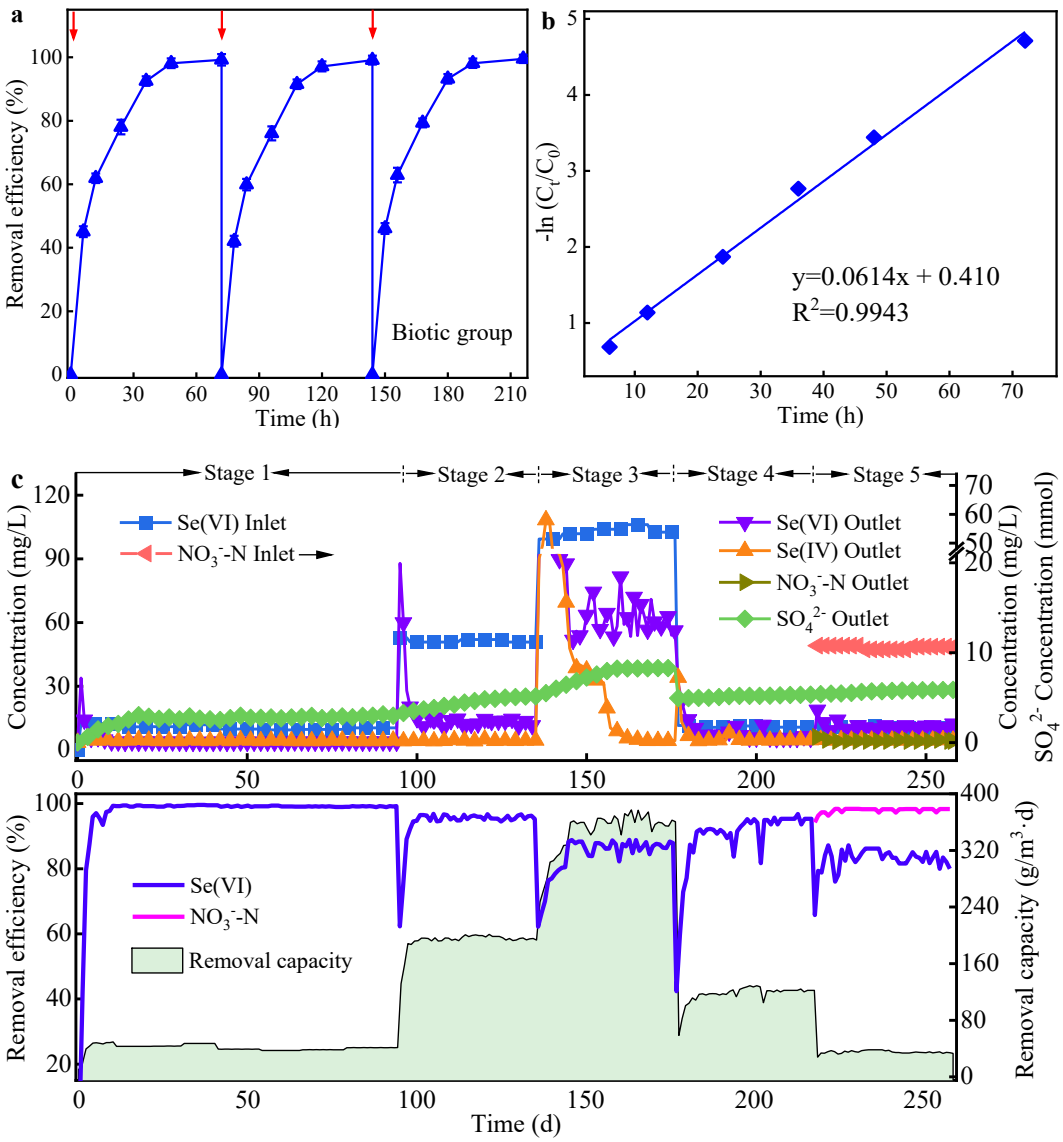

Fig. 1. Se(VI) removal performance in S(0)-driven Se(VI) reduction biosystems. (a) Time histories of Se(VI) removal efficiency during three consecutive operating cycles during batch trial; (b) Pseudo first-order kinetic plots for Se(VI) removal; (c) Time histories of Se(VI), NO_3^--N in influent, Se(VI), Se(IV), NO_3^--N, and SO_4^{2-} in effluent, corresponding Se(VI) and NO_3^--N removal efficiencies, and Se(VI) removal capacities during 258 d operation of the column trial.

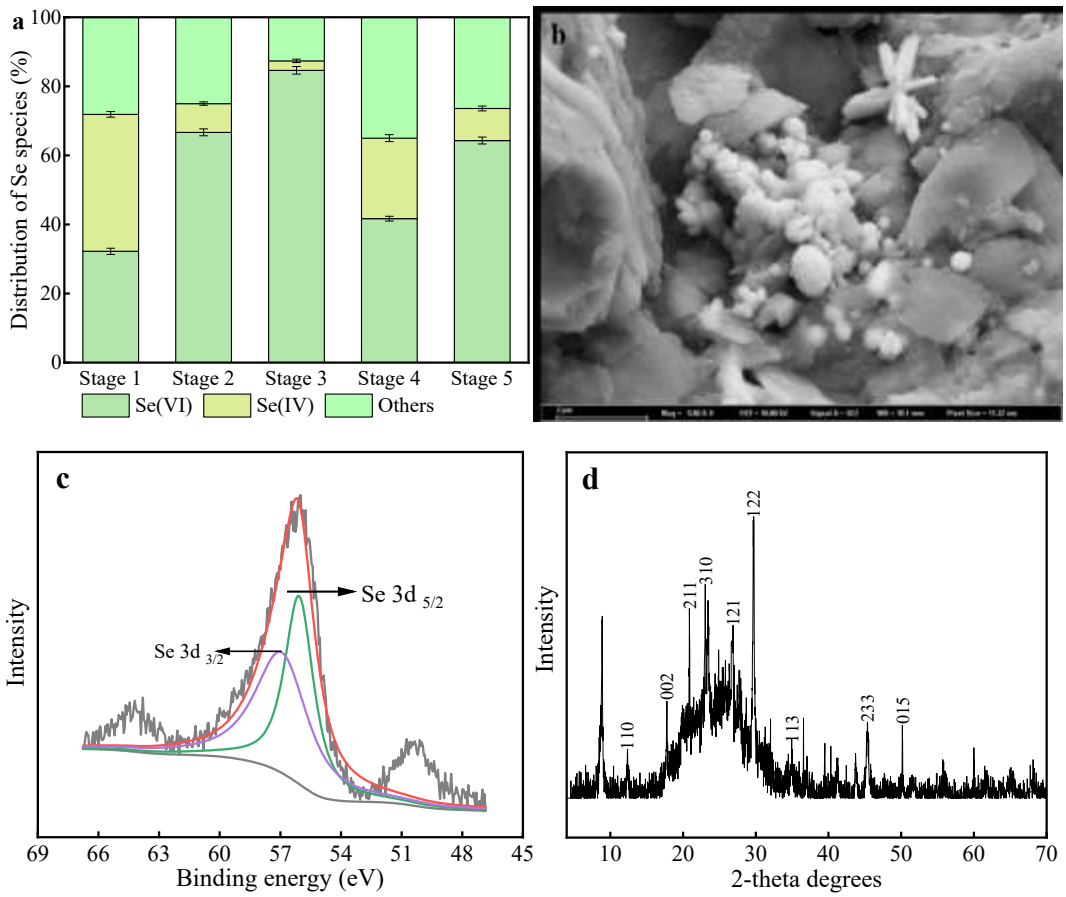

Fig. 2. Characterization of products from Se(VI) bioreduction. (a) Selenium speciation percentages in the effluent. (b) SEM, (c) XPS, and (d) XRD analysis of the precipitates after reaction. SEM: Scanning electron microscope; XPS: X-ray photoelectron spectroscopy; XRD: X-ray diffraction.

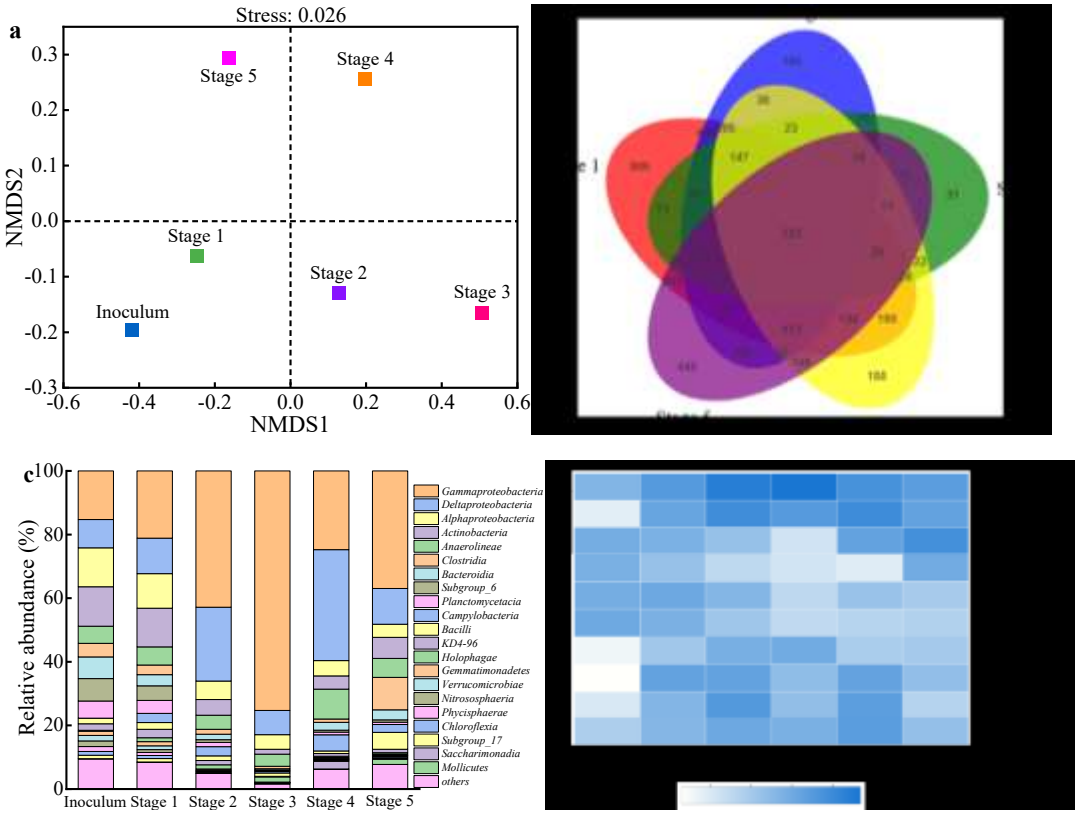

Fig. 3. Microbial community evolution in inoculum and at different stages of column trial. (a) Non-metric multidimensional scaling (NMDS) plot for the distribution of microbial community; (b) Venn plot of microbial richness (b); (c) Class-level relative abundance; (d) Heatmap of functional genera.

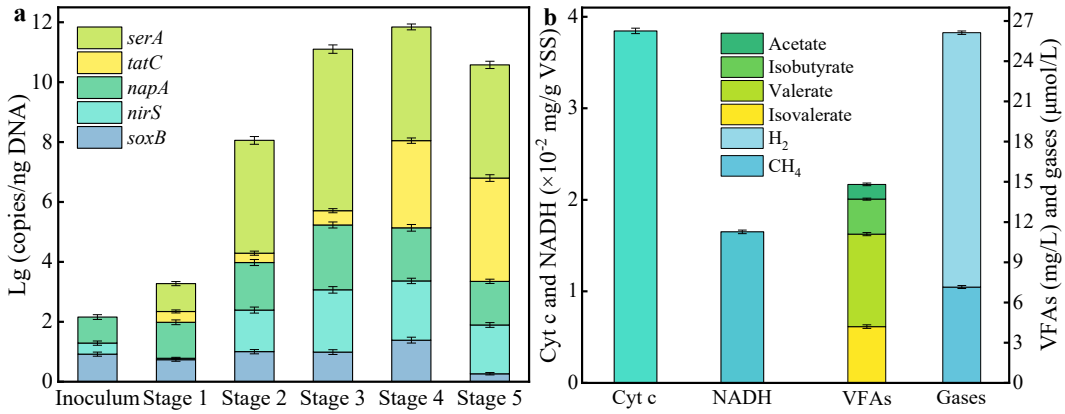

Fig. 4. Metabolic processes of S(0)-driven Se(VI) bioreduction. (a) Abundances of functional genes; (b) Contents of electron transfer compounds and intermediate metabolites. Cyt c: Cytochrome c; NADH: Nicotinamide adenine dinucleotide; VFAs: Volatile fatty acids.

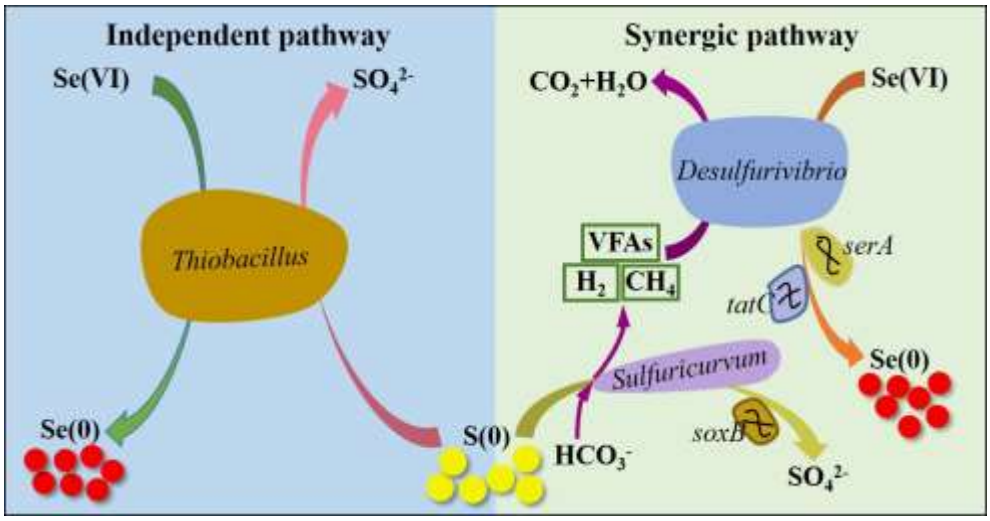

Fig. 5. Mechanistic pathways of microbial Se(VI) reduction processes linked to S(0) oxidation. VFAs: Volatile fatty acids.